LHCb-PUB-2018-004
November 5, 2018

Measurement of the instrumental asymmetry for $K^-\pi^+$-pairs at LHCb in Run 2

A. Davis[1], L. Dufour[2], F. Ferrari[3], S. Stahl[2], J. van Tilburg[4], M. Vesterinen[5]

[1] *Center for High Energy Physics, Tsinghua University, Beijing, China*
[2] *European Organization for Nuclear Research (CERN), Geneva, Switzerland*
[3] *INFN and Università di Bologna, Bologna, Italy*
[4] *Nikhef National Institute for Subatomic Physics, Amsterdam, The Netherlands*
[5] *Department of Physics, University of Warwick, Coventry, United Kingdom*

Abstract

The instrumental asymmetry between $K^-\pi^+$ and $K^+\pi^-$-pairs at the LHCb detector is evaluated using data collected in proton-proton collisions at the LHC at a centre-of-mass energy of 13 TeV in 2015 and 2016. To measure this asymmetry, Cabibbo-favoured $D^+ \to \overline{K}^0\pi^+$ and $D^+ \to K^-\pi^+\pi^+$ decays are used. The efficiency of recording these decay modes has increased with the start of Run-2 data taking. With these improvements the phase-space-integrated $K^-\pi^+$ asymmetry is measured with below-permille statistical precision:

$$A^{\rm det}(K^-\pi^+) = (-0.89 \pm 0.15\,({\rm stat}) \pm 0.06\,({\rm syst}))\% \text{ in 2015},$$
$$A^{\rm det}(K^-\pi^+) = (-1.03 \pm 0.06\,({\rm stat}) \pm 0.06\,({\rm syst}))\% \text{ in 2016}.$$

The dependence of $A^{\rm det}(K^-\pi^+)$ on the kaon momentum is evaluated, along with its sensitivity to the LHCb magnet configuration. Finally, the results are compared with the expected asymmetry determined from the known differences in cross sections of kaons with the detector material. This measurement forms the most precise data-driven determination of the charge bias in the detection of particles at LHCb.

1 Introduction

Measurements of *CP* asymmetries at the LHCb detector continue to show an incredible precision, with statistical and systematic uncertainties in recent charm decays [1] entering the 10^{-4} regime. Such precise measurements of *CP* violation are prone to detector effects which may bias the result. In particular, kaons are known to have charge-asymmetric nuclear cross sections, dependent on the momentum, as illustrated in Fig. 1. Integrating over the typical momenta recorded for kaons in LHCb, mostly ranging from 5 to 45 GeV/c, and the detector material, this cross-section asymmetry introduces an expected relative percent-level difference in the $K^{\pm}$ detection efficiency. Measurements involving kaons therefore rely on a precise calibration of this asymmetry.

Experimentally, access to the combined asymmetry of $K^-\pi^+$ pairs was found to be easier than the single detection asymmetry of charged kaons. This combined asymmetry is defined as the relative difference in detection efficiencies between $K^-\pi^+$ and $K^+\pi^-$-pairs,

$$A^{\text{det}}(K^-\pi^+) = \frac{\varepsilon^{\text{det}}(K^-\pi^+) - \varepsilon^{\text{det}}(K^+\pi^-)}{\varepsilon^{\text{det}}(K^-\pi^+) + \varepsilon^{\text{det}}(K^+\pi^-)}, \tag{1}$$

where $\varepsilon^{\text{det}}(K^{\mp}\pi^{\pm})$ denotes the absolute detection efficiency of $K^{\mp}\pi^{\pm}$ pairs. The detection efficiency not only includes effects from the track reconstruction, but also the (dominant) material interactions. This calibration measurement was already used for measurements of *CP* violation in charm decays [2] in Run 1 of the LHC, covering the data recorded in 2011 and 2012. This note describes a measurement of $A^{\text{det}}(K^-\pi^+)$ using data recorded in 2015 and 2016 at LHCb with an improved selection. The presented approach will be used for the entire data set collected during Run 2 of the LHC, spanning the years 2015 up to and including 2018.

To good approximation, the detection asymmetry between oppositely charged particles can be parametrised solely by their individual four-momenta and origin vertex. As a consequence, the effect of the instrumental asymmetry in a reconstructed decay, e.g. $D_s^+ \to K^-\pi^+\pi^+$, can be decomposed into the detection asymmetries of the separate decay products. This is used to enable a measure of the $K^-\pi^+$ detection asymmetry by taking the difference in the raw asymmetry of two D^+ decay channels,

$$A^{\text{det}}(K^-\pi^+) = A^{\text{raw}}(D^+ \to K^-\pi^+\pi^+) - A^{\text{raw}}(D^+ \to \overline{K}^0\pi^+) - A(K^0), \tag{2}$$

where the raw asymmetry, $A^{\text{raw}}(D^+ \to f)$ is defined as

$$A^{\text{raw}}(D^+ \to f) = \frac{N(D^+ \to f) - N(D^- \to \overline{f})}{N(D^+ \to f) + N(D^- \to \overline{f})}, \tag{3}$$

where N denotes the number of observed decays, and $A(K^0) = -A(\overline{K}^0)$ signifies the correction for regeneration and *CP* violation in the neutral kaon system. The raw asymmetries for both modes decompose as

$$A^{\text{raw}}(D^+ \to K^-\pi^+\pi^+) = A^{\text{det}}(K^-\pi^+) + A^{\text{det}}(\pi^+) + A^{\text{prod}}(D^+) + A^{\text{trigger}} \tag{4}$$

$$A^{\text{raw}}(D^+ \to \overline{K}^0\pi^+) = A(\overline{K}^0) + A^{\text{det}}(\pi^+) + A^{\text{prod}}(D^+) + A^{\text{trigger}}, \tag{5}$$

such that, by subtracting the raw asymmetries of the two D^+ decay modes, the contributions from the production asymmetry, $A^{\text{prod}}(D^+)$, and the trigger asymmetry, A^{trigger}, are

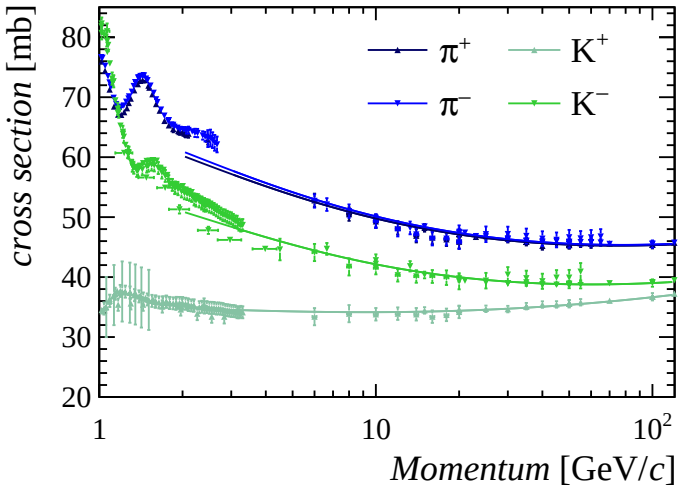

Figure 1: Total cross sections for pions and kaons on a deuterium target, as function of momentum. Data points together with the the overlaid fit function are obtained from Ref. [4].

removed. These asymmetries can be measured accurately, as the D^+ meson is produced abundantly at LHCb [3] and can be separated well from backgrounds.

In this note the general strategy to determine $A^{\rm det}(K^-\pi^+)$ is presented, along with a measurement of $A^{\rm det}(K^-\pi^+)$ in bins of K^- momentum. This is organised as follows. The data selection is explained in Sect. 2, followed by a discussion on the required weighting procedure for the cancellation of any nuisance asymmetries in Sect 3. The extraction of the raw asymmetries is presented in Sect. 4. Section 5 presents the neutral kaon asymmetry, *i.e.* the last term in Eq. 2. After discussing a validation of the method using simplified simulation in Sect. 6, the results from all chapters are combined to $A^{\rm det}(K^-\pi^+)$ and presented in Sect. 7. A comparison of these results with the LHCb simulation is presented in Sect. 8. Finally, the note concludes with an outlook on its relevance to *CP*-asymmetry measurements at LHCb, in particular the measurement of $a^d_{\rm sl}$ [5].

2 LHCb detector and data sample

The LHCb detector [6,7] is a single-arm forward spectrometer covering the pseudorapidity range $2 < \eta < 5$, designed for the study of particles containing b or c quarks. The detector includes a high-precision tracking system consisting of a silicon-strip vertex detector surrounding the pp interaction region, a large-area silicon-strip detector located upstream of a dipole magnet with a bending power of about 4 Tm, and three stations of silicon-strip detectors and straw drift tubes placed downstream of the magnet. The tracking system provides a measurement of momentum, p, of charged particles with a relative uncertainty that varies from 0.5% at low momentum to 1.0% at 200 GeV/c. The minimum distance of a track to a primary vertex (PV), the impact parameter (IP), is measured with a resolution of $(15 + 29/p_{\rm T})$ µm, where $p_{\rm T}$ is the component of the momentum transverse to the beam, in GeV/c. The online event selection is performed by a trigger [8], which consists of a hardware stage, based on information from the calorimeter and muon systems, followed by a software stage, which applies a full event reconstruction.

This analysis uses the data set recorded by LHCb in 2015 and 2016, corresponding to an integrated luminosity of $1.9\,\text{fb}^{-1}$. The protons were colliding at a centre-of-mass energy of 13 TeV. The dipole magnet is essential for the measurement of the charge and momentum of a particle, but also breaks the symmetry between the trajectories of positively and negatively charged particles. As the detection asymmetry of oppositely charged particles explicitly depends on the left-right symmetry in detector performance, the magnet polarity of LHCb is regularly flipped. Averaging data sets over both magnet configurations reduces the asymmetry induced by detector inefficiencies, but the constant variation of detector performance over time breaks the perfect cancellation of this asymmetry, with an expected effect of order 10^{-4} [9]. It is therefore important to quantify the detection asymmetry separately per magnet polarity. In 2015 and 2016, data were recorded with both magnet polarities, corresponding to $0.9\,\text{fb}^{-1}$ with one magnetic field configuration ("magnet up"), and $1.0\,\text{fb}^{-1}$ with the other ("magnet down"). The data sets for 2015 and 2016 were saved using a similar, but not identical, selection. Therefore, the data sets for each year and magnet polarity are therefore analysed separately.

Starting with Run 2, the same reconstruction as offline is ran in the software trigger of LHCb. This allows for offline-quality reconstructed data to be saved in the trigger, stripped of any information unrelated to the selected decay and immediately available for analyses via the so-called Turbo stream [10]. Because of the more efficient use of bandwidth, more D^+ candidates can be recorded by loosening the selection requirements. Most of the candidate selection is implemented in the software trigger. The hardware trigger however could introduce a bias in the charge of the selected decays. Therefore, only D^+ candidates are considered in which the hardware trigger decision was independent of the D^+ decay products. The software trigger itself is again split up in two stages, of which the last stage implements the decay-specific selection for the presented analysis. The first stage requires at least one of the pions originating directly from the D^+ decay to have $p_{\text{T}} > 1.0\,\text{GeV}/c$ and good track quality. This requirement is shared among the two decay modes to mitigate the possible bias in the measured asymmetry. For the $D^+ \to \overline{K}^0\pi^+$ decay mode, this trigger requirement is always applied to the single pion directly originating from the D^+ decay.

In the second stage of the software trigger, candidates consistent with the corresponding decay topologies are reconstructed using tracks with $p_{\text{T}} > 250\,\text{MeV}/c$ and a significant IP with respect to any PV. The reconstructed p_{T} of a D^+ candidate is required to be larger than $2.5\,\text{GeV}/c$. The pions and kaons are distinguished from another by requiring loose particle-identification requirements (PID), based predominantly on information from two ring-imaging Cherenkov detectors [11]. Since 2016, the PID requirements were moved from the online to the offline selection for the $D^+ \to K^-\pi^+\pi^+$ channel to measure their effects on the asymmetry.

Other selection criteria are specific to each decay. For the $D^+ \to K^-\pi^+\pi^+$ candidates a significant flight distance is required, together with a minimum decay time of 0.4 ps (0.5 ps) for 2015 (2016). The tracks selected should have good quality, and at least two tracks should have $p_{\text{T}} > 0.4\,\text{GeV}/c$ ($> 0.2\,\text{GeV}/c$) for 2015 (2016). The reconstructed mass of the $K^-\pi^+\pi^+$ combination is required to lie within 1810 and 1925 MeV/c^2. In 2015, the sum of the transverse momenta of all daughters is required to be larger than $3.0\,\text{GeV}/c$ for the $D^+ \to K^-\pi^+\pi^+$ mode. This condition was relaxed to $> 1.0\,\text{GeV}/c$ for the 2016 data taking, in order to further equalise the D^+ phase-space distributions of the two decay modes. A similar selection is present for the $D^+ \to \overline{K}^0\pi^+$ mode, where the scalar sum of

all transverse momenta is required to be larger than $2.0\,\mathrm{GeV}/c$.

The neutral kaon decay products are separated from other, random pions by requiring a good quality of the reconstructed vertex, together with a minimum $\overline{K}^0$ lifetime of 2.0 ps with respect to the associated PV. By only reconstructing $\overline{K}^0$ in the $\pi^+\pi^-$ final state, one restricts primarily to the decay of the K^0_{S}. The invariant mass of the $\pi^+\pi^-$ combination is required to lie within $50\,\mathrm{MeV}/c^2$ of the K^0_{S} mass [4], and the reconstructed mass of the $K^-\pi^+\pi^+$ combination is required to lie within 1800 and $1935\,\mathrm{MeV}/c^2$. The two pions are required to be reconstructed using hit information from the vertex detector, in addition to the downstream tracking stations. This limits the average decay time of the selected $\overline{K}^0$ to approximately 10% of the K^0_{S} lifetime, and reduces the amount of material traversed. The K^0_{S} candidates which decayed further in the detector are only used to verify the correction of the neutral kaon asymmetry. The background contribution from $\Lambda \to p\pi^-$ decays, in which the proton is mistakenly selected as a pion candidate, is suppressed by particle-identification requirements on both pions originating from the K^0_{S} candidate. This requirement is there only to increase the signal purity, as any (residual) contribution of this background is eliminated by the fit to the three-pion mass, described later in this note.

The D^+ mesons considered are predominantly produced directly in proton-proton collisions (so-called *prompt* decays), as the signal purity is highest for such decays. A selection is applied offline to reduce the sample to prompt candidates only. For the $D^+ \to K^-\pi^+\pi^+$ decays, an additional offline selection aligns the particle-identification requirements on the pion which was selected by the first stage of the software trigger, referred to as the trigger pion, to those of the trigger pion in the $D^+ \to \overline{K}^0\pi^+$ decay mode. If both pions from the $D^+ \to K^-\pi^+\pi^+$ decay caused a positive trigger decision, one is selected randomly. Both modes need to cover the same D^+ phase space, as will be further explained in Sect. 3. Therefore, the D^+ η and p_{T} of the $D^+ \to K^-\pi^+\pi^+$ candidates are required to lie within the boundaries of the $D^+ \to \overline{K}^0\pi^+$ spectrum. The resulting signal purities are high: 85.9% for the $D^+ \to \overline{K}^0\pi^+$ decay mode and 95.3% for the $D^+ \to K^-\pi^+\pi^+$ decay mode.

As the branching fraction of the $D^+ \to K^-\pi^+\pi^+$ decay is very large and the selection efficiency with respect to the $D^+ \to \overline{K}^0\pi^+$ mode is higher, only a quarter of the selected $D^+ \to K^-\pi^+\pi^+$ candidates is saved in the second software trigger stage. This selection is done randomly.

3 Kinematic weighting

The measured asymmetry in D^+ decays is affected by the phase-space-dependent production and detection asymmetries. Different reconstruction efficiencies for both D^+ decay modes cause differences in kinematics, such that residual nuisance asymmetries can remain in the calculation of $A^{\mathrm{det}}(K^-\pi^+)$. Therefore, a per-candidate weighting procedure is applied to mitigate any differences in phase space. The phase space is parametrised by the (p_{T}, η) distribution of the selected D^+ candidates, along with the (p_{T}, η) distribution of the trigger pion.

The (p_{T}, η) spectrum of the $D^+ \to K^-\pi^+\pi^+$ data set varies as a function of kaon momentum, as illustrated in Fig. 2. To measure $A^{\mathrm{det}}(K^-\pi^+)$ as function of kaon momentum, weights need to be assigned as well to the $D^+ \to \overline{K}^0\pi^+$ data set, despite the lower number

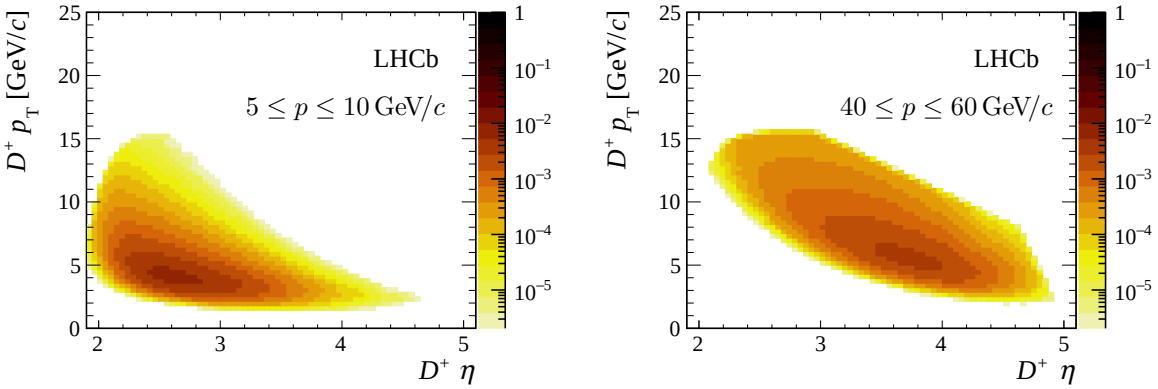

Figure 2: The background-subtracted D^+ (p_T, η) distribution for $D^+ \to K^-\pi^+\pi^+$ candidates in the 2016 magnet up data set for (left) kaon momentum between 5 and 10 GeV/c and (right) kaon momentum between 40 and 60 GeV/c.

of candidates. Three weighting steps are applied to make the most efficient use of the larger $D^+ \to K^-\pi^+\pi^+$ data sample.

In the first weighting step, weights are assigned to the $D^+ \to K^-\pi^+\pi^+$ candidates according to the corresponding D^+ (p_T, η) distribution of $D^+ \to \overline{K}^0\pi^+$ candidates, using a coarse-binned parametrisation. In the second weighting step, weights are assigned to the $D^+ \to \overline{K}^0\pi^+$ candidates, as to match the (p_T, η) distributions of both the trigger pion and the D^+ of the (weighted) $D^+ \to K^-\pi^+\pi^+$ candidates, now using a fine-binned, four-dimensional parametrisation. Lastly, the weighted distributions of the pion's azimuthal angle are equalised, again by assigning weights to the $D^+ \to \overline{K}^0\pi^+$ candidates. Because the azimuthal angle is uncorrelated with the other kinematic variables involved in the previous weighting steps, this does not change the distributions of variables weighted earlier. The weights of all steps are multiplied to obtain the final kinematic weight for each candidate. For clarification, Fig. 3 provides a schematic of the three weighting steps.

4 Signal yield extraction

The $K^-\pi^+\pi^+$ and $\pi^+\pi^-\pi^+$ invariant-mass distributions are used to discriminate between signal and background for the $D^+ \to K^-\pi^+\pi^+$ and $D^+ \to \overline{K}^0(\to \pi^+\pi^-)\pi^+$ data samples, respectively. The weighted, invariant-mass distributions, along with the binned, weighted maximum-likelihood fit results, are shown in Fig. 4 for one bin of K^- momentum. For both decay modes, the signal is modelled as the sum of three Gaussian functions, of which one has a power-law tail on the low-mass side. The means of the Gaussian functions are allowed to vary up to 2.5 MeV/c^2 from each other. Different shape parameters are allowed between D^+ and D^- states, to account for any charge-dependent resolution. The background is modelled using an exponential function, with different slopes for D^+ and D^-. Background-subtracted kinematic distributions, which are required for the weighting steps, are created using the *sPlot* procedure [12], which uses the described fit model. This procedure is repeated for every bin of kaon momentum.

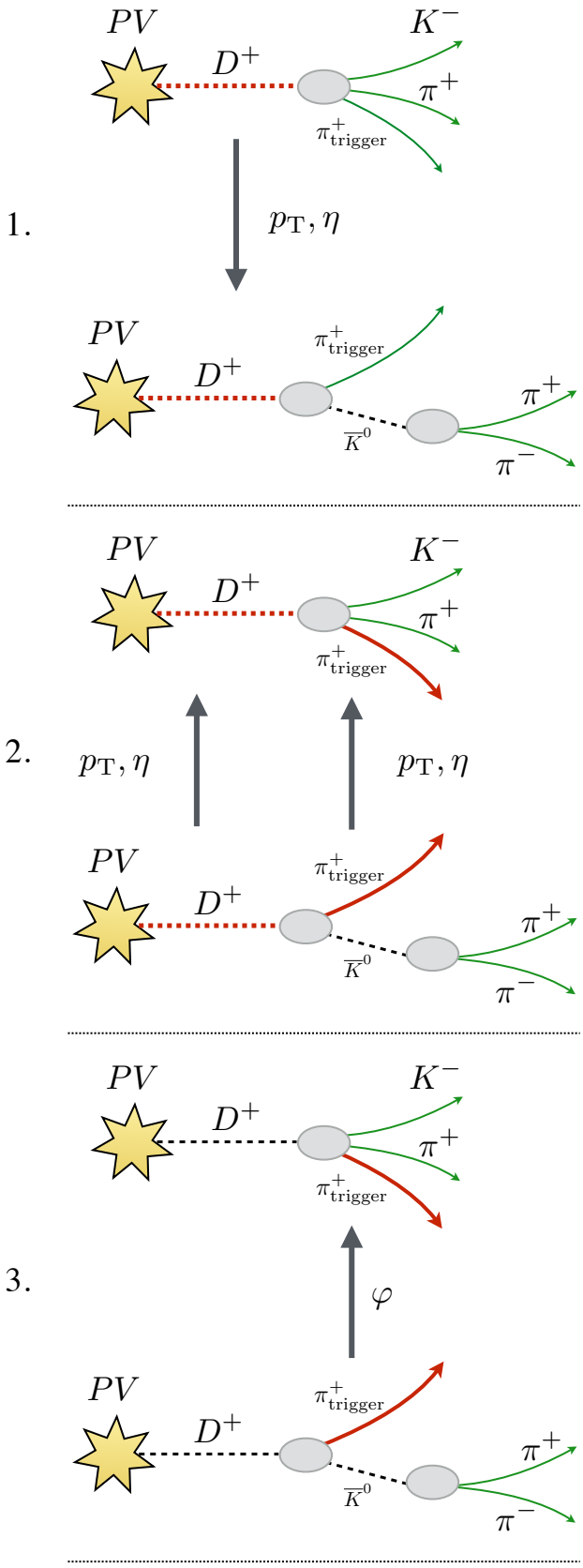

Figure 3: Illustration of the three weighting steps applied to equalise the kinematic distributions between the two D^+ decay modes. The kinematic variables in each step correspond to the track or D^+ candidate highlighted in red.

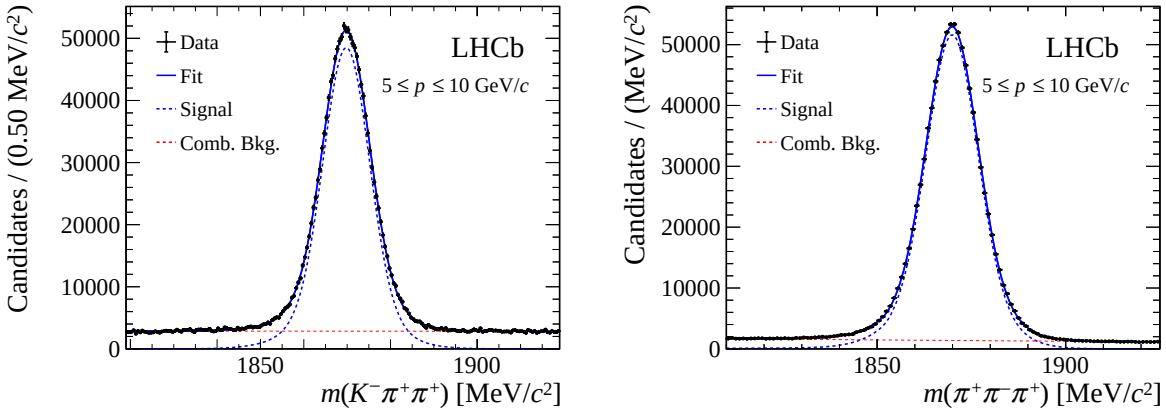

Figure 4: Fits to (left) the weighted $D^- \to K^+\pi^-\pi^-$ invariant mass and (right) the weighted $D^- \to \pi^+\pi^-\pi^-$ invariant mass distributions for kaon momentum between 5 and 10 GeV/c. The data are taken in 2016 with the magnet up polarity.

5 Neutral kaon asymmetry

CP violation in the mixing of neutral kaons, interaction with the detector material (regeneration) and the interference of both effects lead to an additional asymmetry in the selected $D^+ \to \overline{K}^0\pi^+$ decays. The effects from regeneration and *CP* violation are of the same order and same sign in LHCb. The amplitudes are calculated for kaon mixing and *CP* violation, coherently combined with the propagation through the simulated LHCb material. The description of the $\overline{K}^0$ propagation is described in detail in Refs. [13, 14], and only the essential components are repeated here.

Due to its quark content, a K^0 ($\bar{s}d$) can only interact (quasi-)elastically with nucleons composing the detector material, while a $\overline{K}^0$ ($s\bar{d}$) can excite a nucleon into a Λ- or Σ hyperon or associated excited states. This results in a difference in interaction cross sections, which depends on the momentum of the kaon and on the number of nucleons in the detector material, A, and is obtained from Ref. [15],

$$\Delta\sigma = \sigma_T(\overline{K}^0) - \sigma_T(K^0) = 23.2\, A^{0.758}[p(\,\mathrm{GeV}/c)]^{-0.614}\,\mathrm{mb}\,. \tag{6}$$

The difference in interaction cross sections is related via the optical theorem, $\sigma_T = (4\pi/p)\mathrm{Im}f$ to the difference in forward scattering amplitudes $\Delta f = \bar{f} - f$. The phase of Δf is obtained from the phase-power relation as $\arg(\Delta f) = (-124.7 \pm 0.8)^\circ$ [16]. This amplitude difference is used in the description of the time evolution for neutral kaons. The time evolution of the K^0_{L} and K^0_{S} amplitudes which compose an arbitrary neutral kaon state is, modulo a common exponential decay factor, proportional to [14]

$$\alpha_L(t) \propto \alpha_L(0)\cos(\Omega t) - i\frac{\alpha_L(0)\Delta\lambda + \alpha_S(0)\Delta\chi}{2\Omega}\sin(\Omega t), \tag{7}$$

$$\alpha_S(t) \propto \alpha_S(0)\cos(\Omega t) + i\frac{\alpha_S(0)\Delta\lambda - \alpha_L(0)\Delta\chi}{2\Omega}\sin(\Omega t), \tag{8}$$

where the constant $\Omega \equiv \frac{1}{2}\sqrt{\Delta\lambda^2 + \Delta\chi^2}$ is given by the masses $m_{\mathrm{L,S}}$ and decay widths $\Gamma_{\mathrm{L,S}}$

of the $K^0_{\rm L}$ and $K^0_{\rm S}$ states and by the absorption χ ($\bar{\chi}$) of K^0 ($\overline{K}^0$) states through

$$\Delta\lambda = \lambda_{\rm L} - \lambda_{\rm S} = \Delta m - \frac{i}{2}\Delta\Gamma = (m_{\rm L} - m_{\rm S}) - \frac{i}{2}(\Gamma_{\rm L} - \Gamma_{\rm S}) \ ,$$
$$\Delta\chi = \chi - \bar{\chi} = -\frac{2\pi\mathcal{N}}{m}(f - \bar{f}) = -\frac{2\pi\mathcal{N}}{m}\Delta f \ , \tag{9}$$

where $\mathcal{N}$ is the scattering density of the detector material and m the kaon mass. Values of the parameters involved can be found in Table 2 of Ref. [13].

To quantify the impact on the measured $D^+ \to \overline{K}^0\pi^+$ asymmetry, the neutral kaon produced in $D^+ \to \overline{K}^0\pi^+$ decays must first be expressed in the $K^0_{\rm S}$, $K^0_{\rm L}$ basis,

$$|K^0\rangle = \sqrt{\frac{1+|\epsilon|^2}{2}}\frac{1}{1+\epsilon}\left[|K^0_{\rm L}\rangle + |K^0_{\rm S}\rangle\right] \ ,$$
$$|\overline{K}^0\rangle = \sqrt{\frac{1+|\epsilon|^2}{2}}\frac{1}{1-\epsilon}\left[|K^0_{\rm L}\rangle - |K^0_{\rm S}\rangle\right] \ , \tag{10}$$

The neutral kaon amplitude is propagated from the reconstructed D^+ to the reconstructed $K^0_{\rm S}$ decay vertex in the $K^0_{\rm S}$ and $K^0_{\rm L}$ basis using the formulae above, and then projected to its *CP*-even component to extract the relative difference in measured $\pi^+\pi^-$ candidates. The $\overline{K}^0$ candidate is propagated numerically through the simulated detector. For each piece of the flight path of the $\overline{K}^0$, the material type and density are used to modify the amplitudes. The overall asymmetry is calculated by the expected difference in decay rate when assuming a K^0 or $\overline{K}^0$ initial state, averaged over all candidates.

The calculated asymmetry values for the weighted and unweighted samples are given in Table 1. The asymmetry for neutral kaons reconstructed using the nominal selection is slightly larger compared to the integrated value for the Run-1 data set [13], which was determined to be $A(\overline{K}^0) = -A(K^0) = (-0.054 \pm 0.014)\%$. This is mainly due to the looser $p_{\rm T}$ requirements on the signal samples in the software trigger, which results a lower average K^0 momentum, and thus an average larger K^0 decay time. The dominating systematic uncertainty is coming from the estimated 10% uncertainty in the material budget [17]. The uncertainty on the material budget is propagated by varying the simulated material thickness, and re-computing $A(\overline{K}^0)$. The correction is calculated for each bin of K^- momentum separately, and shown in Fig. 5.

The nominal selection for the neutral kaon combines two tracks reconstructed using hits in the vertex detector and the main tracking stations downstream of the dipole magnet, so-called long tracks. The asymmetry is expected to be significantly larger for decays where the reconstructed $K^0_{\rm S}$ vertex lies downstream of the vertex detector ("downstream-reconstructed" candidates), as more material is traversed by the $K^0_{\rm S}$ candidates and these candidates have a larger decay time. Such candidates are not included in the nominal selection described in Sect. 2, but provide a useful input for the estimation of the $\overline{K}^0$ asymmetry as a function of the decay time. The offline selection used for the downstream-reconstructed sample is tighter due to the increased background level. For these candidates, the pseudorapidity of the reconstructed D^+ and $K^0_{\rm S}$ candidates is limited to $\eta < 4.5$. The consistency requirement for the D^+ to originate from a primary vertex is further tightened, and all selected candidates should comply with the desired decay topology when applying a decay chain fit [18]. The resulting expected K^0 asymmetry is included in Table 1. Indeed, the asymmetry of such downstream-reconstructed $K^0_{\rm S}$ candidates is

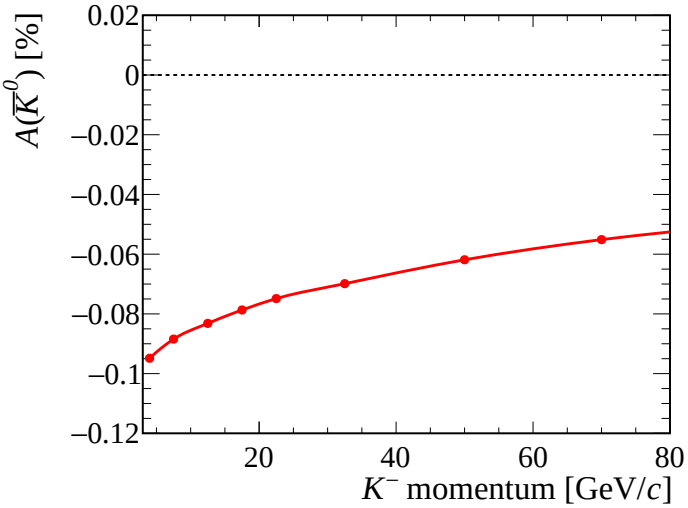

Figure 5: Predicted neutral kaon asymmetry using weights obtained per charged-kaon momentum bin in Sect. 4. The systematic uncertainty from the material uncertainty is not shown as it is fully correlated between bins.

significantly larger than the asymmetry of K^0_S candidates which decay inside the vertex detector ("long-reconstructed" candidates). As this would be a sizeable correction to the charged kaon asymmetry measurement, the downstream sample is only used as a cross-check.

In this cross-check, the raw asymmetries obtained from data and the predicted asymmetries are shown as a function of the K^0_S decay time in Fig. 6 for the long- and downstream-reconstructed samples. The raw asymmetries include an overall offset from the D^+ production and trigger, together with the pion detection asymmetry, while the neutral kaon asymmetry vanishes for zero decay time. This overall offset is accounted for by shifting the prediction with the average difference between raw and predicted asymmetry. Only differences in the shape are of interest for testing the neutral kaon correction. The raw asymmetry follows the predicted downward trend in both samples. The effect is particularly visible in the downstream-reconstructed K^0_S sample.

The amount of traversed material, d, can be expressed in units of the total nuclear interaction length, λ_T. The projection into bins of d/λ_T is shown in Fig. 7. The same

Table 1: Calculated asymmetry $A(\overline{K}^0)$ for different $D^+ \to K^0_S\pi^+$ samples, including systematic uncertainty due to the uncertainty on the material budget. Weighted means that the $D^+ \to K^0_S\pi^+$ momentum spectrum has been weighted to the $D^+ \to K^-\pi^+\pi^+$ kinematics.

Sample	$A(\overline{K}^0)$ [%]	Systematic uncertainty [%]
Nominal selection (long tracks), 2016	−0.1096	0.0057
Nominal selection (long tracks), 2016, weighted	−0.0868	0.0050
Downstream reconstructed, 2016	−0.5271	0.0246

trends are visible, as decay time and flight distance of a K^0_S candidate are correlated. In the projection into bins of the K^0_S decay time material effects are smeared out. Thus, the difference of observed and expected asymmetry in bins of the thickness is more sensitive to a mismodelling of the detector geometry. The detector material is less precisely known than the parameters of *CP* violation in the neutral kaon system. Nevertheless, the agreement is quite good which gives confidence in the correctness of the geometry description and in the predicted asymmetry.

6 Method validation

With the results from Sect. 4 and Sect. 5, one has all the required information to calculate $A^{\rm det}(K^-\pi^+)$ via Eq. 2. What rests however is the validation of Eq. 2. In this Section a partial validation is presented with the use of simulated $D^+ \to K^0_S\pi^+$ and $D^+ \to K^-\pi^+\pi^+$ decays. With the information of the generated particles, one can extract the (simulated) absolute reconstruction efficiency and the corresponding value of $A^{\rm det}(K^-\pi^+)$ with Eq. 1. This asymmetry is then compared to the value extracted from the $D^+ \to K^0_S\pi^+$ and $D^+ \to K^-\pi^+\pi^+$ raw asymmetries by using Eq. 2 to assign a systematic error.

Simulating sufficient decays to achieve a precision comparable to the statistical precision found in data is demanding in terms of computational resources. Therefore, the event simulation is simplified by not generating *pp* collisions, but only D^+ particles which are forced to decay in either of the two considered decay modes. The D^+ $(p_{\rm T}, \eta)$ distribution that is used for this is extracted from $\sqrt{s} = 13\,\text{TeV}$ *pp* collisions generated in PYTHIA [19], with a specific LHCb configuration [20]. Subsequent hadronic decays are described by EVTGEN [21], in which final-state radiation is generated using PHOTOS [22]. The interaction of generated particles with the detector, and its response, are implemented using the GEANT4 toolkit [23] as described in Ref. [24]. The generated samples consist of 100M $D^+ \to K^-\pi^+\pi^+$ events, and 300M $D^+ \to K^0_S\pi^+$ events, where the difference in the generated sample sizes accounts for the lower reconstruction efficiency of the latter mode. A slightly larger sample was created in the magnet up configuration to test

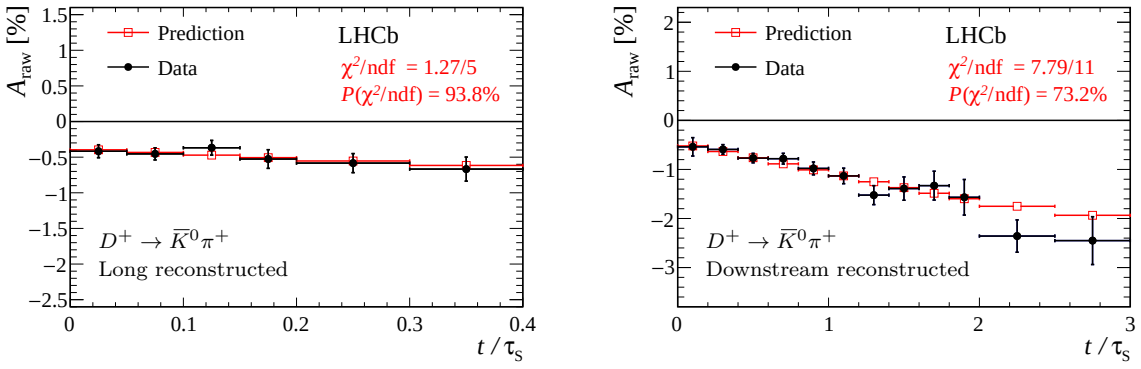

Figure 6: Raw asymmetry of $D^+ \to \overline{K}^0\pi^+$ candidates and the predicted neutral kaon asymmetry as function of the K^0_S decay times for (left) long- and (right) downstream-reconstructed samples. The predicted asymmetry is shifted by the average difference between measured and predicted asymmetry to account for production and other detection asymmetries. The probability for the consistency between data and prediction after the shift is quoted.

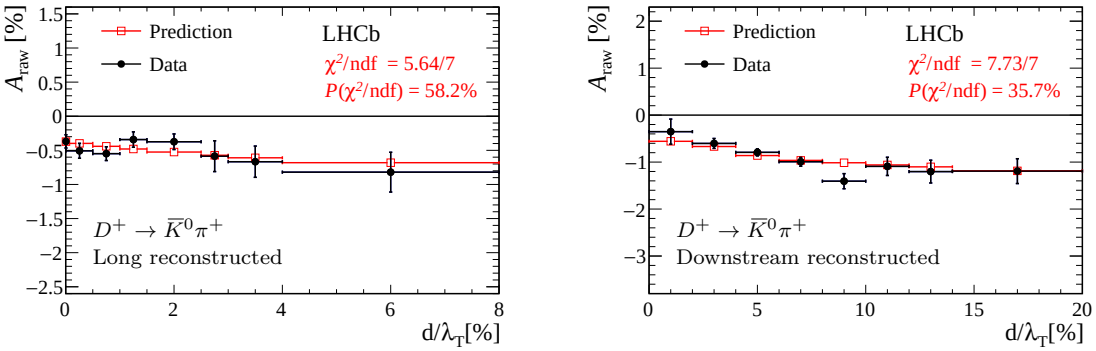

Figure 7: Raw asymmetry of $D^+ \to \overline{K}^0\pi^+$ candidates and the predicted neutral kaon asymmetry as function of the amount of traversed material in nuclear collision lengths for the (left) long- and (right) downstream-reconstructed samples. The predicted asymmetry is shifted by the average difference between measured and predicted asymmetry to account for other detection and production asymmetries.

Table 2: The fitted bias of $A^{\rm raw}(D^+ \to K^-\pi^+\pi^+) - A^{\rm raw}(D^+ \to K^0_S\pi^+)$ with respect to $A^{\rm det}(K^-\pi^+)$ as determined from generator-level information.

Magnet polarity	Fitted bias [%]
Magnet Up	0.04 ± 0.04
Magnet Down	-0.02 ± 0.06
Magnet Average	0.02 ± 0.04

polarity-dependent effects with high precision.

No production or trigger asymmetry is included by the nature of the simplified simulation. The study presented in this section therefore provides a partial validation of Eq. 2. Nevertheless, a preliminary study using simulated proton-proton collisions events shows that the largest contribution to $A^{\rm det}(K^-\pi^+)$ originates from the charge-asymmetric kaon cross sections, which is included. Similarly to the procedure in data, the results are presented in bins of K^- momentum.

Simulated $D^+ \to K^0_S\pi^+$ candidates are assigned per-candidate weights to equalise the π^+ (p_T, η) distributions between the $D^+ \to K^-\pi^+\pi^+$ and $D^+ \to K^0_S\pi^+$ modes for each bin in kaon momentum. As the requirements on the hardware trigger are absent in the fast simulation, one of the pions is chosen randomly. The per-candidate weights are calculated using a forest of shallow decision trees with gradient boosting (a GBDT) [25–27]. The results of $A^{\rm det}(K^-\pi^+)$ computed with Eq. 2 as a function of kaon momentum are shown in Fig. 8. Large differences are visible between the magnet polarities. These differences are explained by simulated left-right differences in the detector.

There is a statistical correlation of $A^{\rm det}(K^-\pi^+)$ between the K^- momentum bins, since the same but differently weighted $D^+ \to K^0_S\pi^+$ candidates are reused. The difference between the two procedures is fitted with a straight line, by using a minimal-χ^2 fit which takes into account the correlation. The resulting bias for each magnet polarity is shown in Table 2. No indication of a bias is found, and Eq. 2 is validated with a precision of 0.06%.

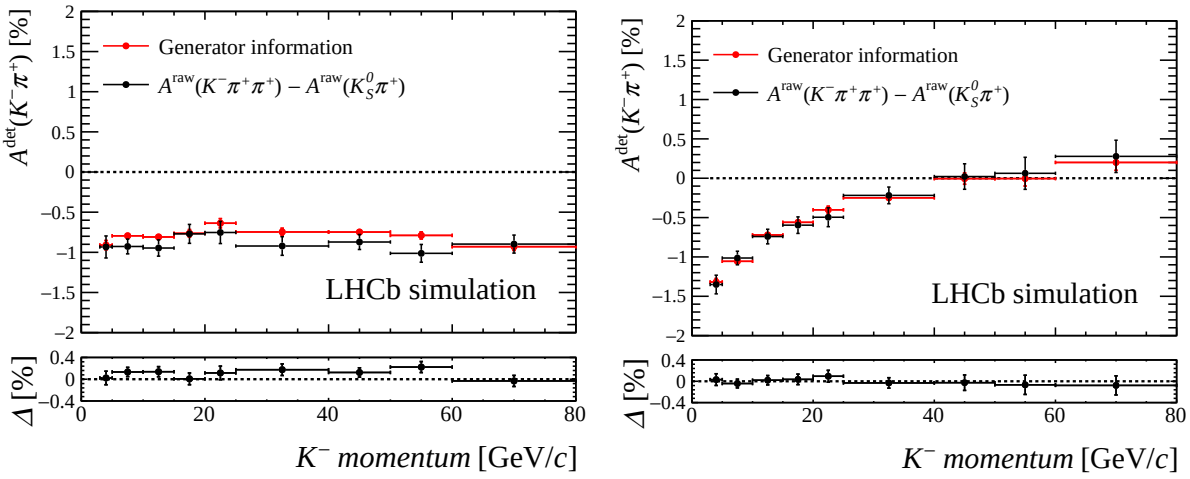

Figure 8: In black, the simulated detection asymmetry resulting from a weighting of the $D^+ \to K^0_S\pi^+$ pion to one of the pions in the $D^+ \to K^-\pi^+\pi^+$ sample in $p_{\rm T}$ and η. In red, the simulated detection asymmetry determined from generator information. The bottom plot shows the difference between the two methods, correcting for the statistical correlation. On the left the results for magnet up are shown, on the right for magnet down.

7 Results

The raw asymmetries are extracted using the binned maximum likelihood fits with the mass models and weights described in Sects. 3 and 4. The raw asymmetries for the $D^+ \to \overline{K}^0\pi^+$ decay mode are then corrected for the neutral kaon asymmetry, using the momentum-dependent values as shown in Fig. 5. The asymmetries in all momentum bins are displayed in Fig. 9. Integrating the asymmetry over K^- momenta $3\,{\rm GeV}/c \leq p \leq 125\,{\rm GeV}/c$, we find

$$A^{\rm det}(K^-\pi^+) = (-0.89 \pm 0.15\,({\rm stat}) \pm 0.06\,({\rm syst}))\% \quad \text{in 2015},$$
$$A^{\rm det}(K^-\pi^+) = (-1.03 \pm 0.06\,({\rm stat}) \pm 0.06\,({\rm syst}))\% \quad \text{in 2016}.$$

The systematic error is the one extracted from the validation on the fast simulation. Small variations in the fixed fit parameters amount to changes in the central value of the order of 0.02%, which is included in the reported statistical error. The numbers are compatible and more precise than those found in Run 1. As expected, the asymmetry decreases as a function of K^- momentum and shows a dependence on the magnet polarity. The increase in statistical precision with respect to Run-1, *i.e.* Ref. [13], is largest for low momenta, and is equivalent to a sample size of up to 3 times larger.

8 Comparison with simulation

The results from Sect. 7 form an excellent measure for the accuracy of the LHCb detector simulation. The dominant contribution to the polarity-averaged value of $A^{\rm det}(K^-\pi^+)$ is due to the charge-asymmetric material interaction of the kaon. Therefore, simulation of the $K^-\pi^+$ asymmetry depends mostly on both the simulated nuclear interaction cross-section asymmetry, as well as the material map of the LHCb detector. To compare

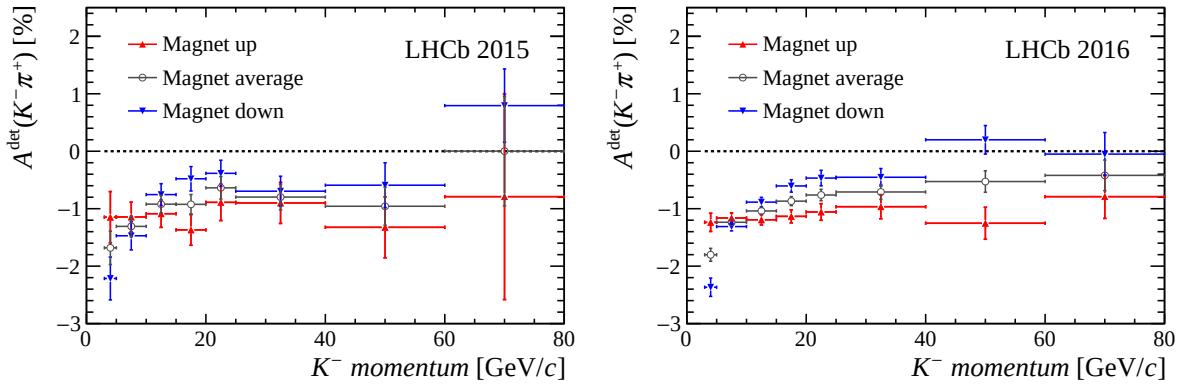

Figure 9: $A^{\rm det}(K^-\pi^+) + A(K^0)$ measured for different kaon momentum bins for (left) 2015 data and (right) 2016 data. There is a statistical correlation between the data points due to the overlap between the $D^+ \to \overline{K}^0\pi^+$ samples used for each bin.

the results from data with simulation, the same simulated $D^+ \to K^-\pi^+\pi^+$ data set is used as was described in Sect. 6. The fast simulation technique used for this data set neglects the underlying event. Large polarity-dependent effects which depend on the event occupancy are expected. Therefore, only the polarity-averaged results are considered in the comparison.

The simulated $D^+ \to K^-\pi^+\pi^+$ candidates are weighted in both K^- $(p_{\rm T}, \eta)$ and π^+ $(p_{\rm T}, \eta)$ kinematics to that of the (weighted) $D^+ \to K^-\pi^+\pi^+$ signal sample for each bin in kaon momentum. The per-candidate weights are calculated using again a GBDT. The resulting magnet-averaged asymmetry is shown in Fig. 10. A relative 10% uncertainty has been added to account for the uncertainty on the simulated material distribution [17]. The results are found to be in good agreement, with a p value of 87.1%, even without the inclusion of the 10% material uncertainty. This indicates that the uncertainty on the material budget likely overestimates this error.

9 Application to physics analyses in Run 2

Due to the strong variation of $A^{\rm det}(K^-\pi^+)$ over phase space, a parametrisation using kaon momentum only is insufficient for high-precision CP-asymmetry analyses. For such analyses, additional weights are assigned to the $D^+ \to K^-\pi^+\pi^+$ candidates to match the π^+ $(p_{\rm T}, \eta)$ and K^- $(p_{\rm T}, \eta)$ distributions to those relevant for the analysis (the target). Due to the limited kinematic overlap between the target and the $D^+ \to K^-\pi^+\pi^+$ decay, the effective statistics available for physics analyses is smaller than the result presented in Sect. 7. Nevertheless, the limiting statistical error often still originates from the $D^+ \to \overline{K}^0\pi^+$ sample.

LHCb has successfully made use of the calibration of $A^{\rm det}(K^-\pi^+)$ to measure CP violation in D^0 decays [13], and to measure the CP asymmetry in mixing for B^0 mesons, $a^d_{\rm sl}$ [5]. The uncertainties of both of these measurements are dominated by the calibration of $A^{\rm det}(K^-\pi^+)$. Improvements in the determination of $A^{\rm det}(K^-\pi^+)$ would therefore directly lead to a gain in precision for these analyses.

The impact of the improvements presented in this note on a measurement of $a^d_{\rm sl}$ is estimated using simulated events. The correction $A^{\rm det}(K^-\pi^+)$ is determined on simulated

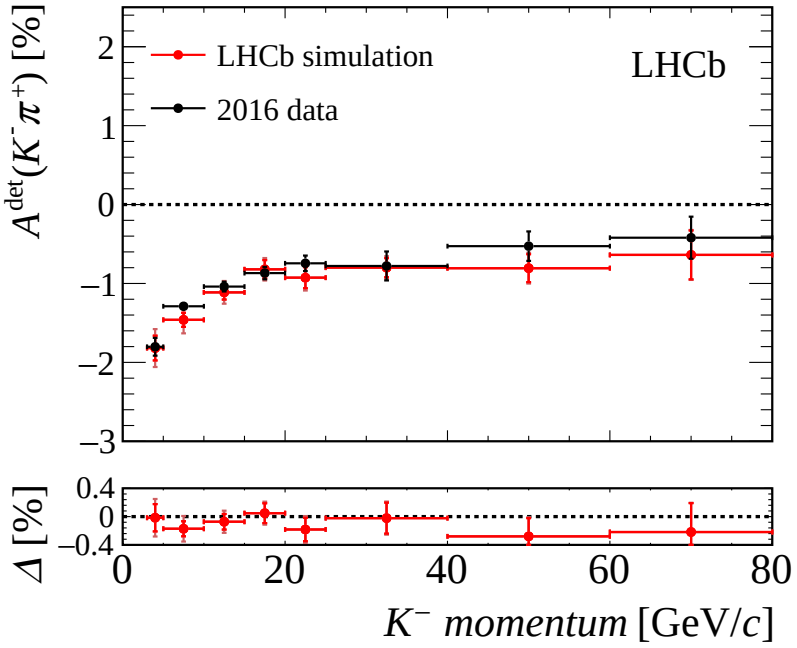

Figure 10: Detection asymmetry for the weighted, fast-simulation samples, with $A^{\rm det}(K^-\pi^+) + A(K^0)$ as extracted from 2016 data superimposed. The red error bars include a 10% uncertainty from the material map.

$B^0 \to D^-\mu^+\nu_\mu$ events, generated in $\sqrt{s} = 8\,\text{TeV}$ and $\sqrt{s} = 13\,\text{TeV}$ proton-proton collisions. A selection which is representative for the analysis is applied to these events, including particle-identification requirements on the final-state hadrons. These requirements are aligned with the calibration samples. For simplicity, only the calibration samples recorded in 2012 (for $\sqrt{s} = 7\,\text{TeV}$) and 2016 (for $\sqrt{s} = 13\,\text{TeV}$) with the magnet down polarity are considered. The weighting strategies for both data sets are kept identical.

The resulting uncertainties are shown in Tab. 3, for both years. The results for 2012 are comparable to those found in the $a^d_{\rm sl}$ analysis. While the recorded luminosity for 2016 is lower than for 2012, the statistical uncertainty for $A^{\rm det}(K^-\pi^+)$ improves from 0.15% to 0.10%. Part of this improvement is attributed to the higher production rate of D^+ mesons [3]. However, the increase in statistical precision is higher than what is expected from the production rate, and is also due to the improved event selection.

The uncertainty of $a^d_{\rm sl}$ increases with approximately twice the uncertainty of $A^{\rm det}(K^-\pi^+)$. Using this approximation, the expected contribution due to $A^{\rm det}(K^-\pi^+)$ to the statistical uncertainty of $a^d_{\rm sl}$ determined on $6\,\text{fb}^{-1}$ of Run-2 data is $\mathcal{O}\,(0.08\%)$. A challenge resides in the control of all systematics, which will require even more precise tests than those presented in Sect. 6.

9.1 Instrumental asymmetry for K^-K^+-pairs

With the use of $A^{\rm det}(K^-\pi^+)$, it is also possible to determine the detection asymmetry of K^-K^+-pairs. This is achieved by calculating the difference between $A^{\rm det}(K^-\pi^+)$ as evaluated for two different target kaons, but with the same target pion. The difference of the resulting two values of $A^{\rm det}(K^-\pi^+)$ result in $A^{\rm det}(K^-K^+)$, as the calibration pion

Table 3: Statistical uncertainties for $A^{\rm raw}(D^+ \to K^-\pi^+\pi^+)$ and $A^{\rm raw}(D^+ \to \overline{K}^0\pi^+)$, determined on data sets weighted to the kinematic distributions of simulated $B^0 \to D^-\mu^+\nu_\mu$ events. Only the data sets recorded with the magnet down polarity were used.

Sample	$\sigma\left(D^+ \to \overline{K}^0\pi^+\right)$ [%]	$\sigma\left(D^+ \to K^-\pi^+\pi^+\right)$ [%]
2012, $\sqrt{s} = 8\,\text{TeV}$, $1.0\,\text{fb}^{-1}$	± 0.13	± 0.07
2016, $\sqrt{s} = 13\,\text{TeV}$, $0.8\,\text{fb}^{-1}$	± 0.09	± 0.04

asymmetry cancels in the difference when one correctly accounts for the correlation between the two results of $A^{\rm det}(K^-\pi^+)$. By the statistical correlation between the two weighted data samples, the statistical uncertainty on the difference, $A^{\rm det}(K^-K^+)$, is significantly smaller than the uncertainty on $A^{\rm det}(K^-\pi^+)$. This weighting strategy was successfully used to control the kaon asymmetry in $D_s^+ \to K^-K^+\pi^+$ decays [28] with a precision of 10^{-4}, and will continue to be used for its Run-2 update.

10 Conclusion

The charge bias in the detection of $K^-\pi^+$-particles at LHCb has been measured using $D^+ \to K^-\pi^+\pi^+$ and $D^+ \to \overline{K}^0\pi^+$ decays. This bias is dominated by the asymmetry in the nuclear interaction rate of the charged kaon, and is of percent-level for the relevant momentum region of $3.0\,\text{GeV}/c \leq p \leq 80.0\,\text{GeV}/c$. Integrated over K^- phase-space and only considering 2016 data, the statistical uncertainty is 0.06% per $1.6\,\text{fb}^{-1}$. The results presented show an improvement in precision with respect to Run 1 due to a higher efficiency of the software triggers and a more efficient use of bandwidth by the Turbo stream. A validation using a simplified simulation technique shows no indication of a bias, with a precision of 0.06%. This ensures the method can be used for the future, high-precision measurements of *CP* violation.

References

[1] LHCb collaboration, R. Aaij *et al.*, *Measurement of CP asymmetry in $D^0 \to K^+K^-$ decays*, Phys. Lett. **B767** (2017) 177, arXiv:1610.09476.

[2] LHCb collaboration, R. Aaij *et al.*, *Measurement of CP asymmetry in $D^0 \to K^-K^+$ and $D^0 \to \pi^-\pi^+$ decays*, JHEP **07** (2014) 041, arXiv:1405.2797.

[3] LHCb collaboration, R. Aaij *et al.*, *Measurements of prompt charm production cross-sections in pp collisions at $\sqrt{s} = 13$ TeV*, JHEP **03** (2016) 159, Erratum ibid. **09** (2016) 013, arXiv:1510.01707.

[4] Particle Data Group, C. Patrignani *et al.*, *Review of particle physics*, Chin. Phys. **C40** (2016) 100001.

[5] LHCb collaboration, R. Aaij *et al.*, *Measurement of the semileptonic CP asymmetry in B^0–$\overline{B}^0$ mixing*, Phys. Rev. Lett. **114** (2015) 041601, arXiv:1409.8586.

[6] LHCb collaboration, A. A. Alves Jr. *et al.*, *The LHCb detector at the LHC*, JINST **3** (2008) S08005.

[7] LHCb collaboration, R. Aaij *et al.*, *LHCb detector performance*, Int. J. Mod. Phys. **A30** (2015) 1530022, arXiv:1412.6352.

[8] R. Aaij *et al.*, *The LHCb trigger and its performance in 2011*, JINST **8** (2013) P04022, arXiv:1211.3055.

[9] M. Vesterinen, *Considerations on the LHCb dipole magnet polarity reversal*, LHCb-PUB-2014-006. CERN-LHCb-PUB-2014-006. On behalf of the LHCb collaboration.

[10] R. Aaij *et al.*, *Tesla : an application for real-time data analysis in High Energy Physics*, Comput. Phys. Commun. **208** (2016) 35, arXiv:1604.05596.

[11] M. Adinolfi *et al.*, *Performance of the LHCb RICH detector at the LHC*, Eur. Phys. J. **C73** (2013) 2431, arXiv:1211.6759.

[12] M. Pivk and F. R. Le Diberder, *sPlot: A statistical tool to unfold data distributions*, Nucl. Instrum. Meth. **A555** (2005) 356, arXiv:physics/0402083.

[13] LHCb, R. Aaij *et al.*, *Measurement of CP asymmetry in $D^0 \to K^-K^+$ and $D^0 \to \pi^-\pi^+$ decays*, JHEP **07** (2014) 041, arXiv:1405.2797.

[14] W. Fetscher *et al.*, *Regeneration of arbitrary coherent neutral kaon states: A new method for measuring the $K^0 - \overline{K}^0$ forward scattering amplitude*, Z. Phys. **C72** (1996) 543.

[15] A. Gsponer *et al.*, *Precise coherent K^0_S regeneration amplitudes for C, Al, Cu, Sn and Pb nuclei from 20 to* 140 GeV/c *and their interpretation*, Phys. Rev. Lett. **42** (1979) 13.

[16] R. A. Briere and B. Winstein, *Determining the phase of a strong scattering amplitude from its momentum dependence to better than 1°: The example of kaon regeneration*, Phys. Rev. Lett. **75** (1995) 402.

[17] LHCb collaboration, R. Aaij *et al.*, *Measurement of the track reconstruction efficiency at LHCb*, JINST **10** (2015) P02007, arXiv:1408.1251.

[18] W. D. Hulsbergen, *Decay chain fitting with a Kalman filter*, Nucl. Instrum. Meth. **A552** (2005) 566, arXiv:physics/0503191.

[19] T. Sjöstrand, S. Mrenna, and P. Skands, *PYTHIA 6.4 physics and manual*, JHEP **05** (2006) 026, arXiv:hep-ph/0603175.

[20] I. Belyaev *et al.*, *Handling of the generation of primary events in Gauss, the LHCb simulation framework*, J. Phys. Conf. Ser. **331** (2011) 032047.

[21] D. J. Lange, *The EvtGen particle decay simulation package*, Nucl. Instrum. Meth. **A462** (2001) 152.

[22] P. Golonka and Z. Was, *PHOTOS Monte Carlo: A precision tool for QED corrections in Z and W decays*, Eur. Phys. J. **C45** (2006) 97, arXiv:hep-ph/0506026.

[23] Geant4 collaboration, S. Agostinelli *et al.*, *Geant4: A simulation toolkit*, Nucl. Instrum. Meth. **A506** (2003) 250.

[24] M. Clemencic *et al.*, *The LHCb simulation application, Gauss: Design, evolution and experience*, J. Phys. Conf. Ser. **331** (2011) 032023.

[25] J. H. Friedman, *Greedy function approximation: A gradient boosting machine*, Ann. Statist. **29** (2001) 1189.

[26] J. H. Friedman, *Stochastic gradient boosting*, Comput. Stat. Data Anal. **38** (2002) 367.

[27] A. Rogozhnikov, *Reweighting with boosted decision trees*, J. Phys. Conf. Ser. **762** (2016) 012036, arXiv:1608.05806.

[28] LHCb collaboration, R. Aaij *et al.*, *Measurement of the CP asymmetry in B_s^0–$\overline{B}_s^0$ mixing*, Phys. Rev. Lett. **117** (2016) 061803, arXiv:1605.09768.